

of the small-scale turbulent modes performed in dynamic current ramp up (CRU) and lower hybrid (LH) heating experiments at FT-2 tokamak using the correlative enhanced scattering technique (CES).

2. The correlative enhanced scattering technique.

The enhanced scattering (ES) or the upper hybrid resonance (UHR) backscattering (BS) technique [15] utilizes for local diagnostics of small-scale plasma fluctuations the effect of growth of wave vector and electric field of the probing extraordinary (X-mode) wave in the UHR, where condition $f_i^2 = f_{ce}^2(R) + f_{pe}^2(r)$ is fulfilled for the probing frequency f_i (R and r are tokamak major and minor radii, f_{ce} and f_{pe} are electron cyclotron and plasma frequencies, correspondingly). To provide the UHR accessibility in tokamak experiment the probing wave is launched from the high magnetic field side of the torus under conditions when the electron cyclotron resonance layer exists somewhere in a plasma. The ES diagnostics benefits of the probing wave field and radial wave number q_r growth leading to high localization, enhanced sensitivity to submillimetric scales and substantial frequency shift of the backscattered wave due to so called Enhanced Doppler effect [11, 16, 17], associated with a finite projection of the large probing wave vector, perpendicular to the UHR surface, onto the poloidal direction in the point shifted from the equatorial plane by y

$$k_\theta = (2k_{\theta^*} + k_r \cos \psi^*)y/y^* \quad (1)$$

here k_{θ^*} is a poloidal wave number out of the UHR at the probing beam axis possessing vertical displacement y^* ; ψ^* is the angle between UHR and magnetic surface there.

The probing and back scattering wave's radial wave numbers k_r and k_{sr} grow rapidly in the vicinity of the UHR. Therefore the back scattering Bragg condition ($q_r = k_r + k_{sr} = 2k_r$) could be easily satisfied for small-scale fluctuations in wide q_r range.

According to [15], the ES frequency spectrum $P_{ES}(\Omega)$ is determined by the turbulence spectrum $|n|_{q_r, q_\theta, \Omega}^2$, ES efficiency $S_{ES}(q_r)$, as well as by the antenna beam power distribution on the UHR surface in the vertical direction $F^2 = \exp[-2(y - y^*)^2 \rho^{-2}]$ and is given by an integral over poloidal and radial fluctuation wave numbers q_θ and q_r

$$P_{ES}(\Omega) = \int I_{q_r, \Omega} dq_r = \int |n|_{q_r, q_\theta, \Omega}^2 S_{ES}(q_r) F^2(y) dq_\theta dq_r, \quad (2)$$

here we also assumed the relation

$$q_\theta = (2k_{\theta^*} + q_r \cos \psi^*)y/y^* \quad (3)$$

between poloidal and radial wave numbers q_θ and q_r of fluctuations contributing to the backscattering in the UHR and vertical displacement y of the point where it happens following from (1) and the BS Bragg condition. The ES technique is only sensitive to fluctuations possessing wavelength smaller than half probing wavelength. The ES efficiency $S_{ES}(q_r)$ shown in FIG.2 for the FT-2 experiment parameters experiences a sharp maximum at $q_r \approx 2(2\pi f_{ce}/c)(c/V_{Te})^{1/2}$ which corresponds to backscattering in the linear conversion point [15]. A significant drawback of the ES diagnostics in the standard approach [15] is poor q_r -resolution, which however may be improved using the correlation technique utilizing

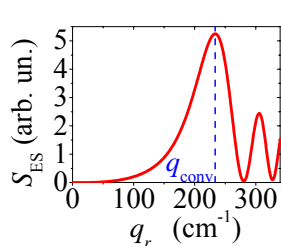


FIG. 2. ES efficiency for $T_e = 90$ eV

simultaneous probing by different frequencies and further correlation analysis of the measured signals [18].

According to [18], the cross-correlation function (CCF) of two ES signals at probing frequencies f_1 and f_2 is related to the ES spectrum $I_{q_r, \Omega}$ via Fourier transform

$$CCF_\Omega(f_1, f_2) = \int I_{q_r, \Omega} \exp\{iq_r [(f_1 - f_2) \partial x_{UH} / \partial f]\} dq_r \quad (4)$$

This relation allows inversion and determination of $I_{q_r, \Omega}$ based on

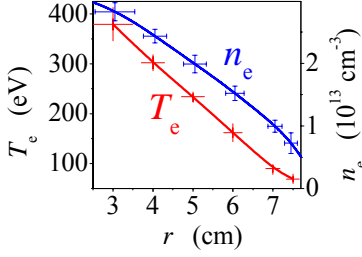


FIG. 3. Electron density and temperature profiles.

experimental data. Moreover, as it was shown in [8], the q_r -spectrum of turbulent fluctuations, as well as their phase velocity may be reconstructed from the CES diagnostics measurement as a result of fitting procedure under natural assumption that the turbulence spectrum is described by expression accounting for the broadening of the drift wave dispersion relation due to nonlinear effects

$$|n|_{q_r, q_\theta, \Omega}^2 = \frac{|n|_{q_r, q_\theta}^2 \sqrt{\pi}}{\Delta q_\theta} \exp \left[- \left(q_\theta - \frac{\Omega}{V_\theta} \right)^2 / (\Delta q_\theta)^2 \right]. \quad (5)$$

3. Two-component ES spectrum investigation in the ohmic discharge.

The experiment was performed in ohmic discharge at the FT-2 tokamak possessing major radius $R_0 = 55$ cm and limiter's radius $a = 7.9$ cm, toroidal field 2.2 T, plasma current 32 kA, density $n_e(0) = 3 \times 10^{19} \text{ m}^{-3}$, electron temperature, measured by multipass Thomson scattering diagnostics, $T_e(0) = 530$ eV. The movable focusing double antennae set, allowing off equatorial plane plasma X-mode probing with the maximal vertical displacement $y_a = \pm 2$ cm was installed at FT-2 at the high magnetic field side [8] (see FIG.1). The beam radius at the UHR position is $\rho \approx 0.7 \div 0.9$ cm, as calculated using the beam tracing code. Both emitting and receiving antennae are narrow along the toroidal direction and thus produce wide toroidal wave number spectra. The probing is performed in the frequency range 53 -72 GHz at low power level of 20 mW. The coupling of emitting and receiving antennae is less than 40 dB.

In the present experiment the probing wave UHR layer was situated at $r > 4$ cm, where necessary condition for the ETG mode excitation $L_T < 1.25 L_n$ following for the FT-2 parameters from analysis [1, 3] was fulfilled (L_T , L_n are electron temperature and density gradient scale lengths). The corresponding T_e and n_e profiles are shown in FIG.3. The ES spectra obtained at $y_a = 1.5$ cm for different probing frequencies (UHR positions) are shown in FIG.4. The ES spectrum is weakly shifted in the electron diamagnetic drift direction and symmetric at the edge, whereas its shift and asymmetry grows, when moving inward. A pronounced "wing" is observable at frequencies less than -2 MHz (HF domain) already at $r = 6$ cm. At $r = 5.6$ cm the second line possessing more than twice higher frequency shift (-2.5 MHz) appears in the spectrum. At $r = 5$ cm its amplitude exceeds the amplitude of the first line. The amplitude of the low frequency (LF) satellite decreases when moving inward the plasma whereas

the high frequency (HF) satellite's amplitude increases. (The non-shifted component in spectrum 4 corresponds to direct coupling of emitting and receiving antennae which appears visible at small ES power.) The observation of a doublet in the ES signal is most likely associated with coexistence of two different drift modes in the FT-2 plasma. To check this supposition and to identify modes the q -spectrum of turbulence was investigated by the CES diagnostics [12]. Two signals at close probing frequencies with difference $|f_2 - f_1| = \{10, 20, \dots, 400\}$ MHz, corresponding to two slightly separated UHR layers in plasma, where the ES by fluctuations with low frequency $\Omega = 2\pi f_\Omega$ occurs, were measured simultaneously using the asymmetric correlation scheme [8]. Probing was performed on the discharge to discharge basis. The

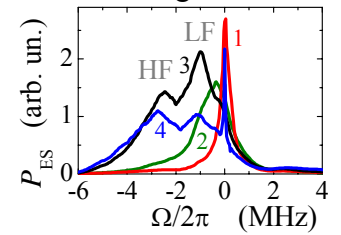


FIG. 4. The ES power spectra P_{ES} for $r = 7.9$ cm (1), 6 cm (2), 5.6 cm (3) and $10P_{ES}$ for 5 cm (4).

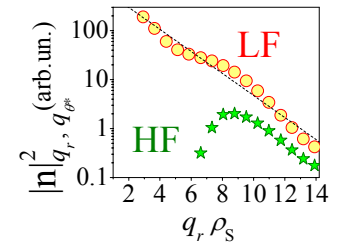


FIG. 5. LF and HF component's q_r spectra.

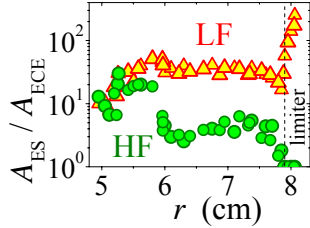


FIG. 6. Normalized LF and HF component amplitudes versus radius.

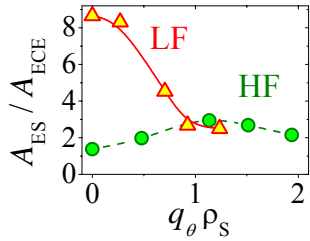


FIG. 7. q_θ dependence of LF and HF components.

data acquisition of the ES signal for all the discharge duration was performed at 20 MHz clock rate of 12-bit ADC. Frequencies higher than 6 MHz were filtered out. Statistical averaging of the data was performed typically over samples of 0.8 ms duration. The reconstructed q_r -spectra for the LF and HF ES frequency spectrum components are shown in FIG.5 in semi logarithmic scale. As it is seen, the LF component spectrum is reconstructed in a wide q_r -domain. It is growing towards small wave numbers and may be well fitted by the linear dependence, whereas the HF component spectrum is localized in the high wave number region. It possesses maximum for scales most easily excited by the ETG instability (at $q_r \rho_s = 8$). The reconstructed poloidal velocity of the HF component directed in the electron diamagnetic drift direction is a factor of 2 higher than the LF component velocity ($V_\theta^{\text{LF}} = 2.7 \pm 0.3$ km/s; $V_\theta^{\text{HF}} = 5.6 \pm 0.5$ km/s). The poloidal wave numbers corresponding to

the LF and HF satellites are $q_\theta^{\text{LF}} = 23 \text{ cm}^{-1}$ and $q_\theta^{\text{HF}} = 27 \text{ cm}^{-1}$. The HF ES signal component radial distribution is different from that of the LF component, as it is seen in FIG.6 where amplitudes of the LF and HF spectral satellites normalized to the ECE emission level are plotted against minor radius. The HF component is growing towards the centre of discharge whereas the LF component is growing in the opposite direction. The dependence of the HF and LF components on the vertical displacement of the antenna set and therefore, according to (1), on the fluctuation q_θ is also different. As it is seen in FIG.7, the HF component is rather growing with q_θ , whereas the LF component is definitely decaying. The differences in the HF and LF ES signal spectral component behavior were also studied in dynamic LH heating experiment.

4. Turbulence evolution in the LH heating experiment.

A different behavior of the UHR BS spectrum LF and HF components was observed in the LH heating experiment at FT-2, where 180 kW of RF power was launched in plasma at frequency 920 MHz during 6 ms initiating transition to the improved confinement regime [19]. The HF component behavior in these dynamical experiments was sensitive to the variation of n_e and T_e profiles. As it is seen in FIG.8a, enhancement of the HF component of the ES spectrum during the LH heating pulse at 30-35.7 ms is only observed for $r < 6.5$ cm when and where the ETG instability condition $L_T < 1.25 L_n$ is satisfied (see FIG.8b). After the

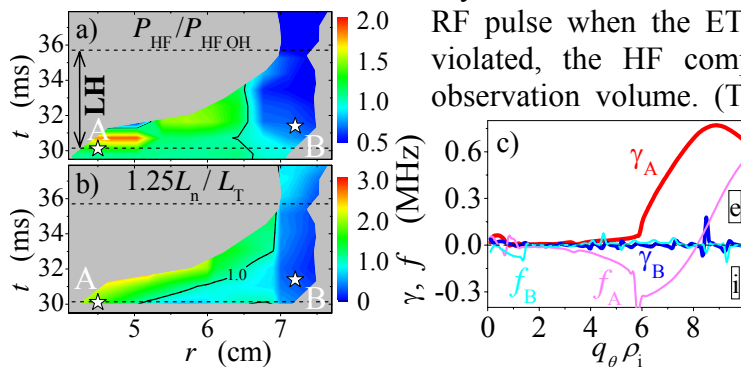


FIG. 8. Evolutions of the (a) HF signal power normalized to its OH value; (b) the ratio of L_n and L_{Te} ; (c) growth rates and frequencies for linear modes at A and B points. (ρ_i - ion gyroradius)

RF pulse when the ETG instability condition is definitely violated, the HF component is suppressed all over the observation volume. (The approximate threshold condition $L_T < 1.25 L_n$ derived in [1, 3] was confirmed for FT-2 experimental parameters using the GS2 code. See for example in FIG.8c the comparison of growth rate dependencies on q_θ computed for points A and B shown in FIG.8b.) This observation provides a final confirmation to the ETG instability origin of the observed

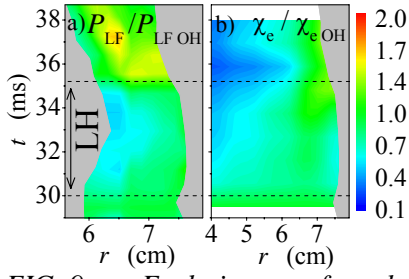


FIG. 9. Evolution of the normalized (a) LF signal power and (b) χ_e .

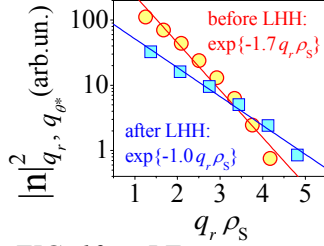


FIG. 10. LF q_r -spectra before and after LHH.

HF turbulence component.

Unlike the HF component, the LF part of the ES signal is not directly sensitive to the relative gradient scale lengths variation. As it is seen in FIG.9, it is rather correlated to the temporal behavior of the effective electron thermal diffusivity χ_e determined from the experimental T_e and n_e profiles with the help of ASTRA transport code. The level of ES signal LF component is decreased simultaneously with χ_e just after the RF power is on. The growth of later at the very edge of plasma preceding the RF pulse termination

is also correlated to the growth of the ES signal observed in this region. It is important to note, that as it was shown by CES technique measurements before and after the RF pulse, the typical q_r of LF fluctuations contributing to the ES signal increased during the pulse. Therefore accounting for the growing dependence of ES efficiency on q_r we may conclude that the growth of the LF component of the ES signal corresponds to even stronger increase in the turbulence level. It is interesting that the q_r -spectra of the LF component plotted in semi logarithmic scale

both before and after the RF pulse, as the spectrum in FIG.5, may be well fitted by the linear dependence (see FIG.10).

These universal exponential spectra of the small-scale LF turbulence component are routinely observed at the FT-2. Evolution of their parameters was studied in the CRU experiment leading to improvement of the energy confinement in the electron channel.

5. Evolution of the exponential turbulence wave number spectra in the CRU experiment.

The measurements were carried out in fast CRU experiment (20 MA/s from 22 kA to 32 kA) (FIG.11). The important feature of this scenario is suppression of anomalous electron transport observed at the current relaxation stage. Namely, investigation of electron and ion temperature, electron density profiles and radiation losses evolution together with ASTRA code modelling allows us to conclude that the effective electron thermal diffusivity coefficient χ_e was suppressed in the discharge at 4-6 ms after CRU and, in particular, decreases by a factor of 2 at plasma periphery. It should be stressed that the χ_e behaviour there (FIG.12) is well correlated with the ES signal suppression by 30-40%. The level of the ES signal LF component power integrated in [-2..+2] MHz frequency band was measured for different

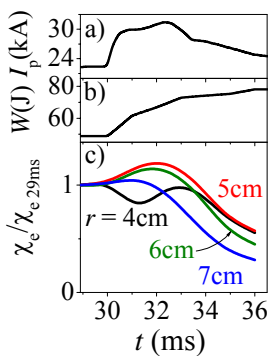


FIG. 11. Dynamics of (a) plasma current, (b) energy content and (c) χ_e .

UHR radial positions from $r = 5.5$ cm till 7.5 cm. The evolution of obtained profiles normalized to the profile at 29 ms (before CRU) is shown in Fig. 12b. (The HF ES signal component “wing” was not pronounced at the plasma edge in the 22 kA discharge.)

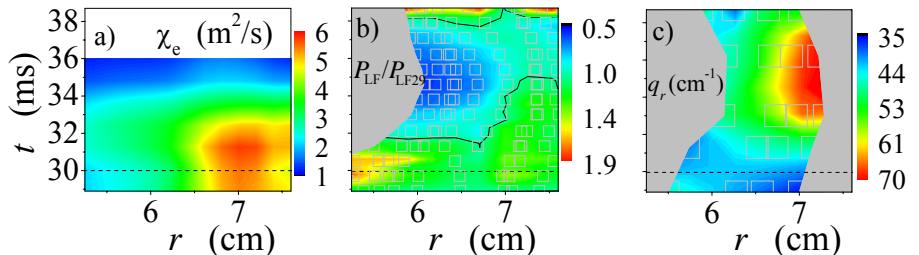


FIG. 12. Temporal variation of profiles (a) χ_e , (b) normalized LF signal power (gray squares: measuring points; solid black curves: $P_{LF}/P_{LF}(29ms)=1$), (c) q_r at ES spectrum maximum.

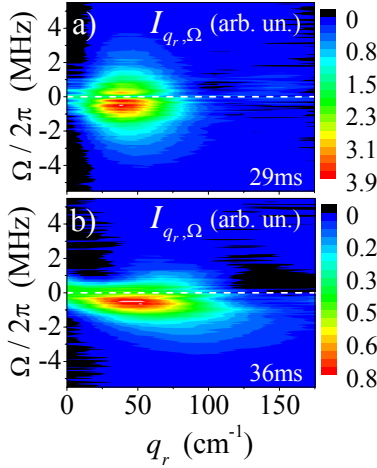


FIG. 13. $I_{q_r, \Omega}$ spectra for (a) 29 and (b) 36 ms in the CRU experiment.

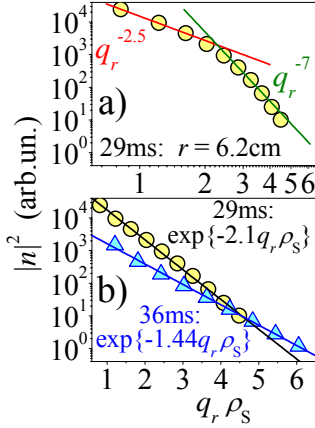


FIG. 14. LF q_r -spectra (a) in double- and (b) semi-logarithmic scale.

Unfortunately, the ES signal suppression could not be directly interpreted in terms of the density fluctuation level drop, because of the strong ($S_{ES} \sim q_r^3$) dependence of the ES efficiency on the turbulence radial wave number. Nevertheless, investigation of the ES $I_{q_r, \Omega}$ spectrum evolution during the CRU experiment provides additional arguments in favour of the turbulence suppression. Namely, as it is clearly seen from comparison of FIG.13a and FIG.13b, the $I_{q_r, \Omega}$ spectrum determined at $r = 6.2$ cm experiences a substantial shift to higher q_r after CRU. The approximation surface $q_r(r, t)$ demonstrating the evolution of q_r values corresponding to ES $I_{q_r, \Omega}$ spectra maximum is shown in FIG.12c. Since the drop of the ES signal (FIG.12b) is accompanied by increase of q_r from 40 cm^{-1} till 70 cm^{-1} (FIG.12c) and thus by strong increase of the ES efficiency, one could conclude that the real drop of the turbulence level was even higher than the ES signal power suppression, observed in the experiment. In addition to the above rough analysis we have also reconstructed the turbulence q_r -spectra at different radii and followed their evolution during CRU. The turbulence q_r -spectra were determined for $8 > q_r \rho_i > 0.8$ at a distance 1-3 cm from the limiter. Plotted in double logarithmic scale (FIG.14a) they are usually knee-like, suggesting that the turbulence cascading to small scales where damping takes place is measured. However when shown in semi logarithmic scale (circles in FIG.14b), they fit linear dependence surprisingly well. Moreover, it was found that in the whole range of radii accessible for ES, during 13 ms after CRU the spectrum could be described by universal dependence $|n|_{q_r}^2 \sim |n|_0^2 \exp\{-q_r L\}$ in the range of 3-4 orders of amplitude (FIG.14b), where $|n|_0^2$ is related to the

turbulence level and L is a typical turbulence scale length. The evolution of these parameters is shown in FIG.15, where $|n|_0^2$ is normalized to its value at 29 ms. Both parameters are found to decrease substantially at 2-6 ms after CRU simultaneously with strong growth of the poloidal plasma rotation velocity gradient in the edge region. Estimated from the ES signal Doppler frequency shift, the later increased from 25 kHz to 190 kHz (FIG.16a).

To interrelate these two effects the linear mode analysis by GS2 code [20] was performed for FT-2 discharge parameters during the CRU experiment allowing to determine the most unstable mode growth rate γ and to compare it with the poloidal plasma rotation shear ω_E at $r = 6.2$ cm. As it is seen in FIG.16b, before CRU (29 ms) the condition $\omega_E \leq \gamma$ is fulfilled in all q -range that makes possible the instability excitation. On contrary, during the current relaxation period (36 ms) the opposite condition $\omega_E > \gamma$ definitely holds for turbulence with $q_{\theta} \rho_i < 1.7$ thus, according to [21], making possible the turbulence suppression at these scales, actually observed in the experiment (FIG. 15a). It should be mentioned that the observed decrease of the turbulence correlation

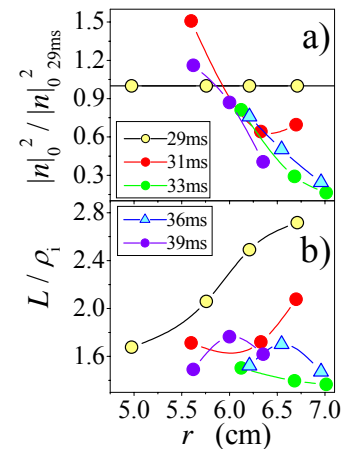


FIG. 15. (a) Turbulence level and (b) spatial scale.

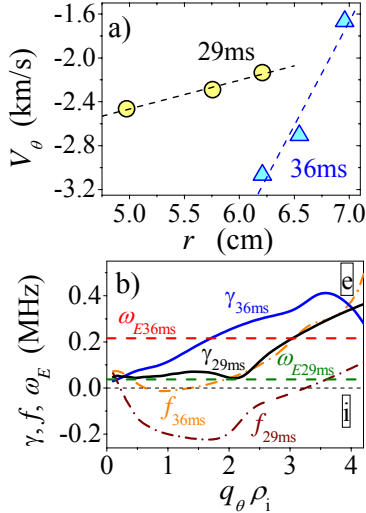


FIG. 16.(a) Poloidal plasma velocity distribution; (b) rotation shear, drift mode growth rate and frequency versus wavenumber.

length (FIG. 15b) accompanying its suppression at $\omega_E > \gamma$ is also predicted by [21]. Based on the domain of $q_\theta \rho_i < 2$ where the LF mode was measured and its sensitivity to the plasma rotation shear we conclude that the mode may be identified as a hybrid of the dissipative TEM [22] and ITG mode.

It is important to note that the drift mode frequencies and phase velocities predicted by the GS2 computation for $q_\theta < 15 \text{ cm}^{-1}$ corresponding to the measured range for the LF component in the CRU experiment are much smaller than actually observed. The difference may be attributed to the plasma cross field drift velocity justifying the procedure of plasma velocity shear determination from the Doppler frequency shift of ES signal used in this paper.

Discussing the physical origin of the universal exponential q -spectrum reconstructed for the LF component one should recall that, according to theoretical predictions [23], the q -spectra of drift wave turbulence in tokamak in a wide q -range corresponding to the so called inertial interval between the high growth rate and high dissipation region should obey a power law taking a Kolmogorov-like form, where q -spectrum looks linear in double logarithmic scale: $\lg(|n_q|^2/|n_{q_0}|^2) = -\alpha \lg(qL)$. Experimental observations carried out in a limited q -range usually confirm this prediction. The measurements specially performed by CO₂ laser scattering in a wide q -range shifted to small scales [24] gave an evidence for a knee-like spectrum composed of two power law spectra with different indexes α . A possible explanation of this observation discussed in [24] is overlapping of the investigated q -range with both inertial interval and turbulence dissipation region. However, as it was shown in [24], when plotted in semi logarithmic scale, the observed spectrum fitted surprisingly well the exponential dependence $\lg(|n_q|^2) \sim -qL$. This intriguing observation performed by CO₂ laser scattering, unfortunately limited in spatial resolution, were appealing for more detailed studies of the small-scale drift turbulence q -spectra by more precise diagnostics. The measurements in the high q_r -range performed in the present paper by the CES technique possessing much better spatial resolution have resulted in confirmation of the exponential spectral law, which is shown to be universal for the LF turbulence component in the FT-2 tokamak plasma. In spite of the fact the measurements are taken at high q_r not typical for the ITG or TEM mode to which the LF mode may be identified, the parameters of its exponential spectrum (level and characteristic length) are shown to be sensitive to the plasma rotation velocity shear and correlated to the electron transport, as it should be for the mentioned modes [23]. A possible explanation of this unconventional spectrum (not predicted by theory treating the nonlinear interaction of drift modes) may be given in terms of the density fluctuation Fourier transform which is provided by any scattering diagnostics. The small-scale asymptotic of this Fourier transform appears to be visible due to high sensitivity of the CES diagnostics in the small-scale domain. This part of the spectrum may not correspond to the fluctuations participating in the energy transfer in the phase space, nevertheless been sensitive to the parameters of the turbulence.

6. Conclusions.

Summarizing the results of the paper we would like to state that two small-scale modes have been found in the enhanced scattering spectra under conditions when the threshold for the

ETG mode instability [1, 3] $L_T < 1.25L_n$ is overcome. The first, identified as the ETG mode, is possessing frequency higher than 2 MHz and radial wave number $q_r \rho_s = 8$ close to the position of the ETG mode growth rate maximum. Its phase velocity is twice as high as for the LF mode and amplitude is growing towards the centre increasing where and when the ETG instability threshold is overcome according to GS2 code, as it is shown in dynamic lower hybrid heating experiment. The second possessing frequency close to 1 MHz is localized at the plasma periphery and probably associated with the small-scale component of the collisional TEM mode. It is found that this turbulence component possesses a wide q -spectrum which could be described by universal exponential dependence in the range of 3-4 orders of amplitude characterized by two parameters – the turbulence level and scale length. Both parameters are found to decrease substantially during the dynamic current ramp up discharge when the shear of the poloidal plasma rotation increases at plasma periphery exceeding the growth rate of drift instability determined with the GS2 code. Simultaneously transition to the improved confinement resulting in suppression of anomalous electron transport is observed in the experiment.

Financial support of RFBR Grants 07-02-00895, 08-02-00989, 08-02-00610, RFBR – NWO Centre of excellence Grant 047 018.2006.007, INTAS Grant 05-8046 and “Russian Science Support Foundation” is acknowledged.

- [1] Mikhailovskiy A.B. 1967 *Sov. J. Tech. Phys.* **37** 1365
- [2] Jenko F., Dorland W., Kotschenreuther M. and Rogers B.N. 2000 *Phys. Plasmas* **7** 1904
- [3] Jenko F., Dorland W. and Hammett G.W. 2001 *Phys. Plasmas* **8** 4096
- [4] Lin Z. et al. 2004 *Proc. 20 IAEA Conf. on Fusion Energy* (Vienna) IAEA-CN/TH/8-4
- [5] A. Bottino et al. 2006 *Proc. 33 EPS Conference on Plasma Phys.* (Rome) ECA 30I O-3.001
- [6] J. Candy and R.E. Waltz 2006 *Proc. 21 IAEA Conf. on Fusion Energy* (Chengdu) IAEA-CN/TH/2-1
- [7] Gusakov E.Z., Gurchenko A.D., Altukhov A.B. et al. 2005 *Proc. 32 EPS Conf. on Control. Fusion and Plasma Phys.* (Tarragona) ECA 29C D-4.007
- [8] E.Z. Gusakov, A.D. Gurchenko, A.B. Altukhov et al. 2006 *Plasma Phys. Control. Fusion* **48** A371
- [9] Rhodes T.L. et al. 2006 *Proc. 21 IAEA Conf. on Fusion Energy* (Chengdu) IAEA-CN/EX/P4-37
- [10] J.E. Menard et al. 2006 *Proc. 21 IAEA Conf. on Fusion Energy* (Chengdu) IAEA-CN/OV2-4
- [11] E.Z. Gusakov, A.D. Gurchenko, A.B. Altukhov et al. 2006 *Plasma Phys. Control. Fusion* **48** B443
- [12] A.D. Gurchenko, E.Z. Gusakov, A.B. Altukhov et al. 2007 *Nucl. Fusion* **47** 245
- [13] T.L. Rhodes, W.A. Peebles, J.C. DeBoo et al. 2007 *Plasma Phys. Control. Fusion* **49** B183
- [14] E. Mazzucato, D.R. Smith, R.E. Bell et al. 2008 *Phys. Rev. Lett.* **101** 075001
- [15] Novik K.M., Piliya A.D., 1994 *Plasma Phys. Control. Fusion* **35** 357
- [16] Bulyiginskiy D.G. et al. 2001 *Phys. Plasmas* **8** 2224
- [17] Altukhov A.B., Gurchenko A.D., Gusakov E.Z. et al. 2003 *Proc. 30 EPS Conf. on Control. Fusion and Plasma Phys.* (St.-Petersburg) ECA 27A P-4.170pd
- [18] Gusakov E.Z., Kaganskaya N.M., Kramer M. and Selenin V.L. 2000 *Plasma Phys. Control. Fusion* **42** 1033
- [19] Lashkul S.I. et al. 2006 *Proc. 21 IAEA Conf. on Fusion Energy* (Vienna) IAEA/EX/P6-18
- [20] M. Kotschenreuther, G. Rewoldt, W.M. Tang 1995 *Comp. Phys. Comm.* **88** 128
- [21] H. Biglari, P.H. Diamond, P.W. Terry 1990 *Phys. Fluids B* **2** 1
- [22] J.W. Connor, R.H. Hastie, P. Helander and A.Field 2006 *Proc. 33 EPS Conf. on Plasma Phys.* (Rome) ECA 33I O-3.002
- [23] W. Horton 1999 *Rev. Mod. Phys.* **71** 735
- [24] P. Hennequin et al. 2004 *Plasma Phys. Control. Fusion* **46** B121